Enhancing the relative capture width of submerged point absorbers

Boyin Ding Nataliia Sergiienko Fantai Meng
Benjamin Cazzolato Maziar Arjomandi Peter Hardy

April 28, 2016

Abstract

Point absorbers are one of the most common wave energy converters due to their simplicity, however, they are typically inefficient. A single tether point absorber, despite oscillating with multiple degrees of freedom, extracts energy primarily from heave motion only, limiting relative capture width to a third of the maximum possible. This paper will explore methods of harvesting energy from multiple oscillation modes to maximise relative capture width of a point absorber. Two variants of the point absorber design are investigated; a single tether buoy with an asymmetric mass distribution, and a buoy with three tethers in tripod formation. The behaviour of the point absorbers will be explored from a modal perspective using eigenanalysis. It will be shown that if properly designed, both variants can produce relative capture width two to three times that of the traditional heaving point absorber.

1 Introduction

Ocean waves are a vast resource of renewable energy, with recent estimates suggesting a global potential exceeding 2 TW [1]. In comparison with wind and solar energy, ocean waves have a much higher power density and are more predictable [2]. Despite the fact that there are more than 200 different wave energy converters (WECs) in various stages of development [3], WEC technology is still in its pre-commercial phase [4]. Many concepts of extracting energy from ocean waves have been realised, with more than a thousand WEC designs being patented by 1980 [5], but none of them have demonstrated their advantage over others. Floating and fully submerged point absorbers comprise a great proportion of existing full-scale WEC prototypes [6]. Such devices typically operate offshore in deep water waves with higher energy content [7]. Oscillating wave energy absorbers, depending on their relative dimensions and position to the propagating wave, can be categorised as [7]

(i) Terminator - a device which operates perpendicular to the wave propagation direction;

(ii) Point absorber - a device with dimensions much smaller than the length of incoming waves;

(iii) Attenuator - a device oriented parallel to the wave direction and with length larger than that of the dominant wave.

Point absorbers are generally designed as axisymmetric buoys which are inherently insensitive to wave direction [8]. Axisymmetric WECs have been thoroughly studied by [9, 10, 11], where it has been shown that maximum power absorption is a function only of wavelength and WEC oscillation modes, and not dependent on WEC size. The maximum power available to a point absorber oscillating in various modes is displayed in Table 1 considering linear potential theory and unrestricted WEC motion. It is apparent that an axisymmetric body needs to oscillate in at least two modes (one radiating symmetric waves and the other radiating antisymmetric waves [12]) to absorb the maximum available energy from waves. Consequently, generic heaving point absorbers can only absorb one third of the total available energy. Point absorbers are typically connected to a power-takeoff (PTO) unit via a single tether, as shown in Figure 1. In practice point absorbers are free to oscillate in heave, surge and pitch modes. However, the majority of the power is absorbed from the heave mode only due to kinematic constraint of the single tether PTO (e.g. PTO is aligned along heave mode for most of the time). Hence, power absorption capability is limited to one third of the maximum possible.

Table 1: Maximum absorbed power ($P_{\max}$) by an axisymmetric body, where λ represents wave number and J represents energy transport of the wave per unit width of wave frontage. [12]

Mode	**Maximum power,** $P_{\max}$
Heave	$(\lambda/2\pi)J$
Surge and heave	$(3\lambda/2\pi)J$
Surge, sway and heave	$(3\lambda/2\pi)J$
Surge and pitch	$(\lambda/\pi)J$
Surge, heave and pitch	$(3\lambda/2\pi)J$

This paper will study methods of harvesting energy from multiple oscillation modes to maximise the absorption capability of a point absorber. Two variants of the generic point absorber design are investigated; a single tether buoy with an asymmetric mass distribution that aims to enhance the coupling between the surge and heave mode, and a buoy with three tethers in tripod formation that aims to ensure effective kinematic coupling between the oscillation modes and the PTO units. The point absorbers are assumed to be fully submerged in both cases. WEC behaviour will be explored from a modal perspective using eigenanalysis. Linearized models of the point absorber variants will be described in Section 2, followed by an eigenanalysis of the WECs in Section 3. The results of the eigenanalysis will be discussed in Section 4, along with a performance

comparison between devices. Results will be presented in the frequency domain.

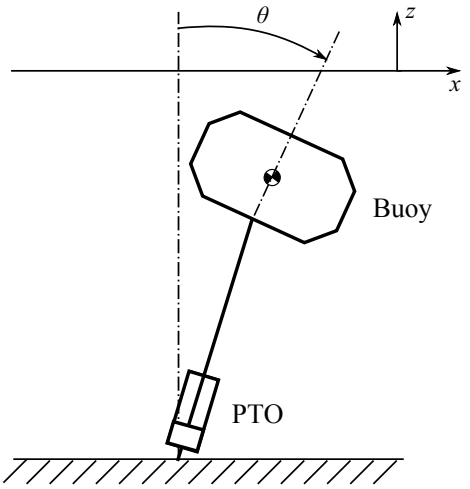

Figure 1: Schematic of a generic single tether fully submerged point absorber

2 Background Theory

This section describes the characteristics of the point absorbers considered, as well as the linearization of their mathematical models for eigenanalysis. Spherical buoys are used in this study given their simple geometries, particularly for the ease of investigation on the asymmetric mass point absorber. This study is restricted to monochromatic plane waves and linear wave theory. Therefore, the dynamics of the point absorbers can be simplified as the planar case with three degree of freedom (DoF) motion (namely surge, heave, and pitch).

2.1 Generic Single Tether Point Absorber

The equation of motion of a floating or submerged body in monochromatic waves has been derived by Cummins [13]:

$$(\mathbf{M} + \mathbf{A}_\infty)\ddot{\mathbf{x}} + \int_0^t \mathbf{K}_{rad}(t-\tau)\dot{\mathbf{x}}(\tau)d\tau + \mathbf{F}_{h/stat} = \mathbf{F}_{exc} + \mathbf{F}_{pto}, \qquad (1)$$

where $\mathbf{x}$ is a vector of 6 DoF motion of the WEC centre of mass, $\mathbf{M}$ is a mass matrix, $\mathbf{A}_\infty$ is the hydrodynamic added mass existing at infinite frequency, $\mathbf{K}_{rad}(t)$ is a retardation function, and $\mathbf{F}_{h/stat}$, $\mathbf{F}_{exc}$ and $\mathbf{F}_{pto}$ are the hydrostatic, wave excitation and PTO forces exerted on the body respectively.

Assuming that waves propagate unidirectionally along the x-axis as shown in Figure 1, WEC motion will be two-dimensional. Consequently, only the surge, heave and pitch modes need to be considered in the analysis, meaning the 6

DoF displacement vector can be reduced to $\mathbf{x} = [x \quad z \quad \theta]^\intercal$, indicating surge displacement, heave displacement and pitch angle respectively. As the buoy is fully submerged, the generalised hydrostatic force is $\mathbf{F}_{h/stat} = [0 \quad (\rho V - m)g \quad 0]^\intercal$, where ρ is the density of water, m and V are the mass and volume of the buoy respectively, and g is the gravitational acceleration.

Modelling the PTO mechanism as a linear spring-damper system, the PTO force that acts on the tether attachment point on the buoy along the tether is:

$$F_{pto} = (-C_{pto} - B_{pto}\Delta\dot{l} - K_{pto}\Delta l), \tag{2}$$

where $-C_{pto} = -(\rho V - m)g$ is a pretension force in the tether to counteract the buoyancy/hydrostatic force, K_{pto} and B_{pto} are the PTO stiffness and damping respectively, Δl is the dynamic change in the overall tether length from equilibrium due to PTO extension.

Equation (1) can be linearised at the nominal buoy position, $\hat{\mathbf{x}} = (0, 0, 0)$, at which point the tether is vertical, assuming small angular motions of the system and mapping the change in the tether length to the Cartesian coordinates of the body. Thus, the linearised frequency domain model of the generic point absorber with spherical buoy can be written as [14]:

$$(\mathbf{M} + \mathbf{A}(\omega))\,\hat{\ddot{\mathbf{x}}} + (\mathbf{B}_{pto} + \mathbf{B}(\omega))\,\hat{\dot{\mathbf{x}}} + \mathbf{K}_{pto}\hat{\mathbf{x}} = \hat{\mathbf{F}}_{exc}, \tag{3}$$

where

$$\mathbf{M} = \begin{pmatrix} m & 0 & 0 \\ 0 & m & 0 \\ 0 & 0 & I_y \end{pmatrix}, \quad \mathbf{A}(\omega) = \begin{pmatrix} a_{11} & 0 & 0 \\ 0 & a_{33} & 0 \\ 0 & 0 & 0 \end{pmatrix}, \quad \mathbf{B}(\omega) = \begin{pmatrix} b_{11} & 0 & 0 \\ 0 & b_{33} & 0 \\ 0 & 0 & 0 \end{pmatrix},$$

$$\mathbf{K}_{pto} = \begin{pmatrix} \frac{C_{pto}}{l_0} & 0 & -\frac{C_{pto}a}{l_0} \\ 0 & K_{pto} & 0 \\ -\frac{C_{pto}a}{l_0} & 0 & \frac{C_{pto}a}{l_0}(l_0 + a) \end{pmatrix}, \quad \mathbf{B}_{pto} = \begin{pmatrix} 0 & 0 & 0 \\ 0 & B_{pto} & 0 \\ 0 & 0 & 0 \end{pmatrix}, \tag{4}$$

where m is the mass of the buoy, I_y is the moment of inertia of the buoy in the pitch axis, a_{ii} and b_{ii} represent hydrodynamic coefficients of the buoy at its nominal pose, l_0 denotes the initial/nominal tether length, a is the radius of the buoy, which defiens the distance from the geometric centre of mass of the buoy to the attachment point of the tether on the buoy hull. The $\hat{}$ symbol represents the complex amplitudes associated with frequency domain. The total effective mass matrix is the sum of the buoy mass matrix $\mathbf{M}$ and the hydrodynamic added mass matrix $\mathbf{A}(\omega)$. The PTO stiffness matrix $\mathbf{K}_{pto}$ is dependent on the tether nominal length, PTO stiffness, tether pretension force, and distance between the buoy centre-of-mass and tether attachment point on the buoy. $\mathbf{B}_{pto}$ only depends on the PTO damping coefficient. In theory, nominal tether length can be changed by varying the height of the mooring base. With a proper design, the impact of mooring base structure to the buoy hydrodynamic coefficients is negligible.

At the nominal position the following 1x3 inverse Jacobian matrix maps the Cartesian space velocities of the buoy to tether elongation velocity,

$$\Delta\dot{l} = \mathbf{J}^{-1} \begin{pmatrix} \dot{x} \\ \dot{z} \\ \dot{\theta} \end{pmatrix} = \begin{pmatrix} 0 & 1 & 0 \end{pmatrix} \begin{pmatrix} \dot{x} \\ \dot{z} \\ \dot{\theta} \end{pmatrix}. \tag{5}$$

2.2 Asymmetric Mass Point Absorber

There have been a few attempts to use an asymmetric body shape to increase the power absorption capability of point absorbers [15]. However, to the best knowledge of the authors, there are no systematic studies available that provide design guidelines for an asymmetric shaped buoy. This is mainly due to the fact that asymmetric shaped buoys have more design parameters and more complex hydrodynamic behavior in comparison to the generic symmetric shaped buoy. Therefore, a generic spherical buoy with an uneven mass distribution is considered, as an attempt to understand if a beneficial coupling between oscillation modes can be achieved via mass-offset.

Figure 2 illustrates the proposed asymmetric mass point absorber. A point mass m_2 is placed on the spherical buoy with mass m_1 and radius a. The location of the point mass is defined by the mass offset, r_{gy}, and the offset angle, φ. The nominal pose of the buoy (rotated by ϕ from the initial pose of the generic case) is calculated to balance the torques arising from the weight of the offset mass and the pretension force on the tether. Based on the calculated nominal pose, the dynamics of the asymmetric mass point absorber can be linearized to the same form shown in Equation (3) as given by Equation (6). The linearization process is described in detail in the Appendix.

$$\mathbf{M} = \begin{pmatrix} m_1 + m_2 & 0 & m_2 r_{gy} \sin(\varphi) \\ 0 & m_1 + m_2 & -m_2 r_{gy} \cos(\varphi) \\ m_2 r_{gy} \sin(\varphi) & -m_2 r_{gy} \cos(\varphi) & I_y \end{pmatrix},$$

$$\mathbf{A}(\omega) = \begin{pmatrix} a_{11} & 0 & 0 \\ 0 & a_{33} & 0 \\ 0 & 0 & 0 \end{pmatrix},$$

$$\mathbf{B}(\omega) = \begin{pmatrix} b_{11} & 0 & 0 \\ 0 & b_{33} & 0 \\ 0 & 0 & 0 \end{pmatrix},$$

$$\mathbf{K}_{pto} = \begin{pmatrix} C_{pto}/l_0 & 0 & -C_{pto} a \cos(\phi)/l_0 \\ 0 & K_{pto} & K_{pto} a \sin(\phi) \\ -C_{pto} a \cos(\phi)/l_0 & K_{pto} a \sin(\phi) & \begin{pmatrix} C_{pto} a \cos(\phi)(1 + a\cos(\phi)/l_0) \\ -m_2 g r_{gy} \sin\varphi + K_{pto} a^2 \sin^2(\phi) \end{pmatrix} \end{pmatrix},$$

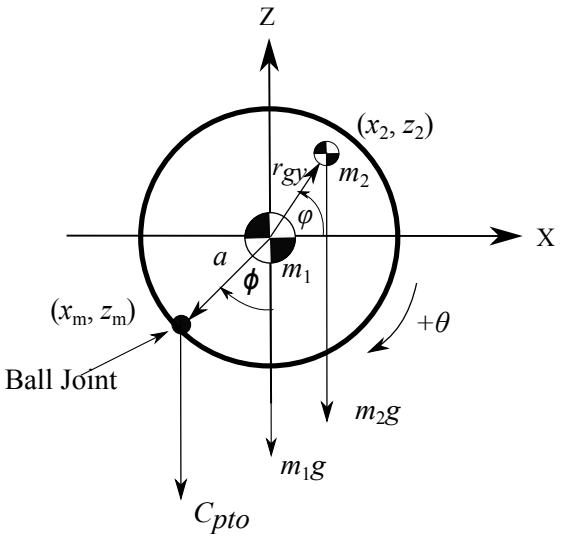

Figure 2: Asymmetric mass point absorber at nominal pose for linearization.

$$\mathbf{B}_{pto} = \begin{pmatrix} 0 & 0 & 0 \\ 0 & B_{pto} & B_{pto}a\sin(\phi) \\ 0 & B_{pto}a\sin(\phi) & B_{pto}a^2\sin^2(\phi) \end{pmatrix}. \tag{6}$$

In comparison to the generic single-tether case, both heave-pitch and surge-pitch couplings are enhanced as evident in the buoy mass matrix $\mathbf{M}$, as well as the PTO stiffness $\mathbf{K}_{pto}$ and damping $\mathbf{B}_{pto}$ matrices. At the nominal pose, the Cartesian space velocities of the buoy are mapped to the tether elongation velocity via the inverse Jacobian

$$\Delta\dot{l} = \mathbf{J}^{-1} \begin{pmatrix} \dot{x} \\ \dot{z} \\ \dot{\theta} \end{pmatrix} = \begin{pmatrix} 0 & 1 & a\sin(\phi) \end{pmatrix} \begin{pmatrix} \dot{x} \\ \dot{z} \\ \dot{\theta} \end{pmatrix}. \tag{7}$$

2.3 Three Tether Point Absorber

The three-tether WEC was firstly studied by Srokosz [16], showing the ability to absorb three times more power than a generic heaving buoy with a single tether. In the current analysis it is assumed that all three tethers are connected to individual power take-off systems, allowing the WEC to generate power from heave, surge and pitch motion modes. The tethers are equally spaced around the WEC, as shown in Figure 3, in order to provide insensitivity of the system to the direction of wave propagation. The inclination angle of the tethers plays an important role in the WEC design as it defines the contribution of each motion mode in the total power absorption. It has been found by the authors [17] that

for the spherical buoy, the tethers should be perpendicular to each other, forming edges of the cuboidal vertex to provide maximum power generation, and that the variation of the tether angle within several degrees from the optimal solution has a negligible effect on the power output of the system. In the current analysis it is assumed that all three PTO systems have identical control parameters (stiffness and damping), which makes the WEC insensitive to the direction of wave propagation. However, it should be noted that having individual control over all three tethers may slightly improve the power absorption of the buoy while increasing a complexity of the control system design.

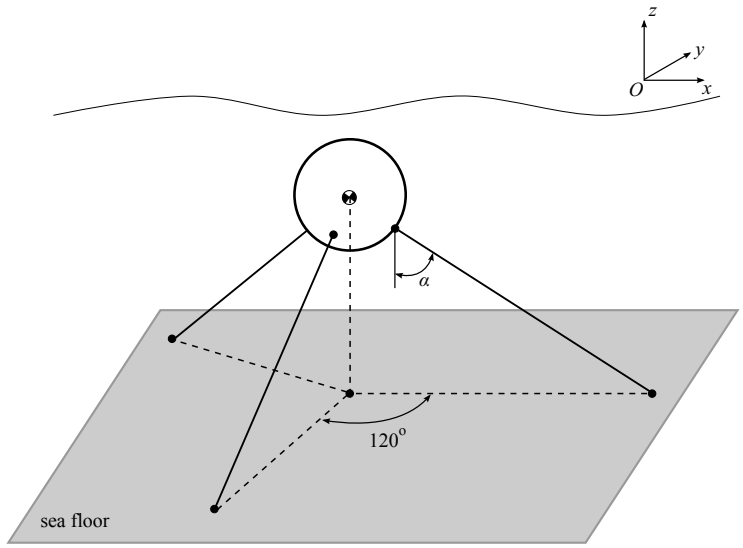

Figure 3: Schematic showing the three-tether point absorber propotype

The full derivation of the motion equations for the three-tether WEC has been presented in [18, 19] and will not be repeated in this paper. Taking into account that all tethers point toward the centre of mass of the buoy at the nominal pose and are inclined to the vertical at the angle α, the linearised frequency domain model of the three-tether WEC can be described by Equation (3), where

$$\mathbf{K}_{pto} = \begin{pmatrix} \frac{3\sin^2\alpha}{2}\left(K_{pto} - \frac{C_{pto}}{3l_0\cos\alpha}\right) + \frac{C_{pto}}{l_0\cos\alpha} & 0 & -\frac{C_{pto}a}{l_0} \\ 0 & 3\cos^2\alpha\left(K_{pto} - \frac{C_{pto}}{3l_0\cos\alpha}\right) + \frac{C_{pto}}{l_0\cos\alpha} & 0 \\ -\frac{C_{pto}a}{l_0} & 0 & \frac{C_{pto}a(l_0+a)(\cos^2\alpha+1)}{2l_0\cos\alpha} \end{pmatrix},$$

$$\mathbf{B}_{pto} = \begin{pmatrix} \frac{3}{2} B_{pto} \sin^2 \alpha & 0 & 0 \\ 0 & 3B_{pto} \cos^2 \alpha & 0 \\ 0 & 0 & 0 \end{pmatrix}, \tag{8}$$

$\mathbf{M}$, $\mathbf{A}(\omega)$, and $\mathbf{B}(\omega)$ are defined in Equation (4). In comparison to the generic single-tether case, the PTO stiffness matrix $\mathbf{K}_{pto}$ is also dependent on the tether angle. Hence, PTO stiffness is effectively coupled into the surge mode.

The buoy velocities in a Cartesian coordinate frame are mapped to the rate of change in the tether length through the inverse kinematic Jacobian, which at the nominal buoy position can be described as:

$$\begin{pmatrix} \Delta \dot{l}_1 \\ \Delta \dot{l}_2 \\ \Delta \dot{l}_3 \end{pmatrix} = \mathbf{J}^{-1} \begin{pmatrix} \dot{x} \\ \dot{z} \\ \dot{\theta} \end{pmatrix} = \begin{pmatrix} -\sin \alpha & \cos \alpha & 0 \\ \frac{\sin \alpha}{2} & \cos \alpha & 0 \\ \frac{\sin \alpha}{2} & \cos \alpha & 0 \end{pmatrix} \begin{pmatrix} \dot{x} \\ \dot{z} \\ \dot{\theta} \end{pmatrix}. \tag{9}$$

3 Eigenanalysis

In this section, the eigenanalysis on the linearised models of the point absorber variants is presented. The real eigenvectors and eigenvalues are calculated from the stiffness and total effective mass matrices for each case, which represent the mode shapes and natural frequencies of the oscillating modes respectively. Each oscillating mode consists of a linear combination of the three fundamental Cartesian motions of the buoy, namely heave, surge, and pitch, as illustrated in Figure 4. Based on these characteristics, the behavior of the system can be better understood from a modal perspective. For a fair comparison between the cases, all three cases use a spherical point absorber with a 5m radius, and are assumed to be submerged at 7m below the water surface in sea water of 50m depth. The buoy mass has been set to be half of the displaced water mass, resulting in a net buoyancy force equivalent to the force on the buoy due to gravity. For the asymmetric mass buoy, the total buoy mass is equally divided into two parts; the "sphere mass"and a "offset mass"placed at r_{gy}=5m and $\varphi = -30°$. The location of the point offset mass is chosen so that the moment of inertia of the asymmetric mass buoy and the generic buoy have the same order of magnitude. The fixed parameters used for eigenanalysis are shown in Table 2. Optimization of system variables (e.g. PTO stiffness and damping, tether length and angle) are conducted on the linearized frequency-domain models for various incident wave frequencies. The tether stroke is not constrained during optimization in this section.

Table 2: WEC fixed parameters used in the study.

Parameter	**Value**
Buoy shape	sphere
Radius, a	5 m
Submergence depth (to buoy centre of buoyancy)	7 m
Water depth	50 m
Buoy mass to displaced water mass ratio	0.5
Mass offset for asymmetric mass buoy	r_{gy}=5 m; $\varphi = -30°$
Sphere mass to point offset mass ratio, m_1/m_2	1

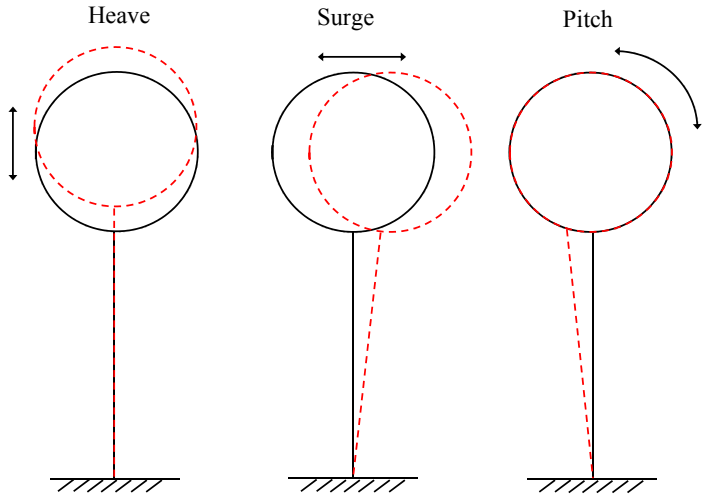

Figure 4: Cartesian/buoy-space motions of buoys. Left: heave, middle: surge, right: pitch.

3.1 Generic Single Tether Point Absorber

For the generic single-tether point absorber case, at the nominal pose the optimal PTO stiffness, being the control parameter that maximises power absorption, is dependent only on incident wave frequency and independent of tether length. The eigenvectors and eigenvalues are calculated from the stiffness and mass matrices shown in Equation (4), where the optimal PTO stiffness is obtained for each wave frequency. The tether length has been varied from 1 to 10 times the buoy radius to illustrate the effect this has on the modal behaviour, despite not affecting the power for this generic case. Figure 5a shows the variation in natural frequency of various oscillation modes versus tether length to buoy radius ratio for an incident wave frequency of $\omega = 0.45$ rad/sec, where

mode 1 represents a surge-dominant mode, mode 2 represents a pitch-dominant mode, and mode 3 represents a heave-dominant mode. The natural frequency of the heave-dominant mode is approximately equal to the incident wave frequency of 0.45 rad/sec and is independent of the tether length, as expected. The natural frequency of the surge-dominant mode decreases with the increase in tether length due to the fact that surge-dominant mode is governed by the pendulum motion of the buoy-tether system. It is clear that at a tether length to buoy radius ratio of $l_0/a = 3.5$, the natural frequencies of surge-dominant mode and heave dominant mode are equal, which means maximum wave power can be absorbed in the Cartesian space of the buoy. The natural frequency of the pitch-dominant mode is considerably higher than the normal incident wave frequency range and therefore is not shown here. The variation of the eigenvectors for each oscillation mode (modal components in Cartesian space of the buoy) with tether length to buoy radius ratio, l_0/a, are displayed in Figure 5b. It is clear that the eigenvectors of the coupled modes (e.g. off-diagonal terms in the eigenvectors) are much smaller in magnitude than the eigenvectors of te dominant modes (e.g. diagonal terms in eigenvectors), meaning oscillation modes oscillation modes are only loosely coupled. Figure 5c shows the normalized contributions to the tether velocity from each mode. It can be seen that due to kinematics, only the motion of heave-dominant mode is efficiently transformed into tether elongation. Hence, only one third of the total/available power in the wave can be absorbed by the generic single tether point absorber.

Figure 6a and 6b respectively show the optimal natural frequencies of the modes and the optimal tether length to buoy radius ratio against a range of feasible incident wave frequencies. The PTO setting as well as the tether length (that maximises the power absorption) are optimized for the frequency-domain model given by Equation (3) for each wave frequency, with an initial tether length of 3.5m and an initial PTO setting optimal for the heave mode only (given by $\sqrt{\frac{K_{pto}}{m + a_{33}}}$ =wave frequency, ω and $B_{pto} = b_{33}$). It can be seen that the natural frequency of pitch-dominant mode is always out of the possible incident wave frequency range. The natural frequency of heave-dominant mode is roughly equal to the incident wave frequency for the entire frequency range, hence resonance of the heave mode can always be achieved by optimising PTO settings. The natural frequency of surge-dominant mode is almost constant for the entire wave frequency range, arising from an almost constant tether length. From Figure 6b, it is clear that the "optimal"tether length to buoy radius ratio remains approximately unchanged from the initial value provided to the optimisation solver. This is not surprising given that the surge dominant mode does not effectively couple into the tether elongation as evident in Equation (5), and therefore, the solver used for the optimisation of power (fminsearch in Matlab) does not change the tether length from its initial starting value.

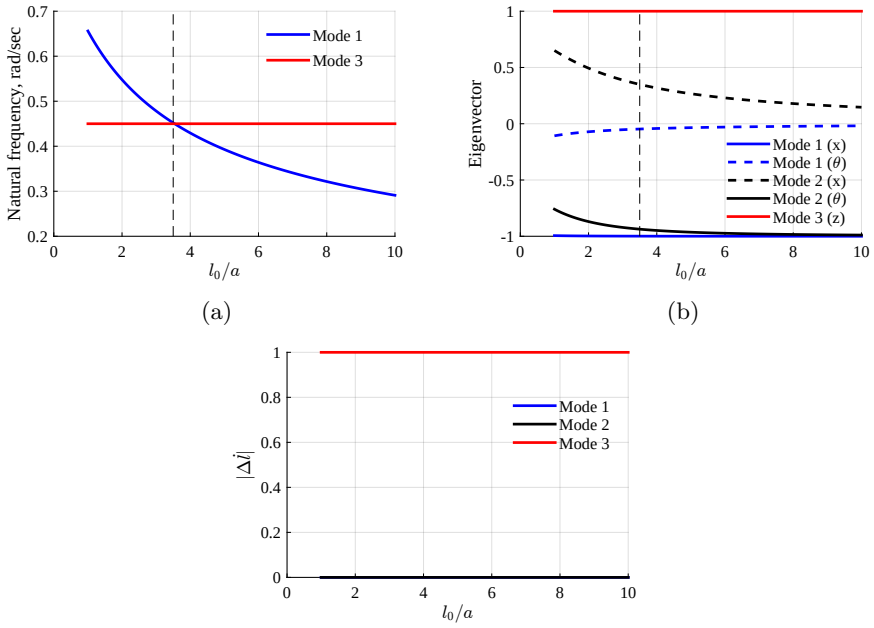

Figure 5: Eigenanalysis of the generic single-tether WEC vs. tether nominal length for one incident wave frequency of $\omega = 0.45$ rad/sec: (a) Natural frequencies (eigenvalues) of buoy Cartesian space modes in rad/s; (b) Corresponding mode shapes (eigenvectors); (c) contribution of the buoy Cartesian space modes to the tether velocity, $|\Delta \dot{l}|$.

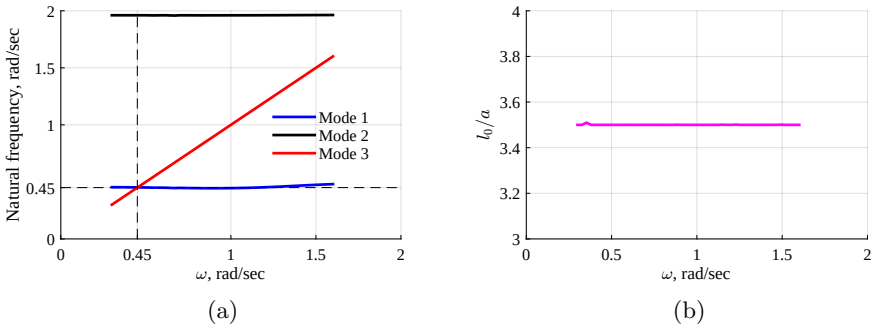

Figure 6: (a) Natural frequencies (eigenvalues) of the generic single-tether WEC against a range of incident wave frequencies at optimal conditions (optimal PTO setting and optimal nominal tether length for each frequency); (b) Optimal tether length to buoy radius ratio against incident wave frequencies.

3.2 Asymmetric Mass Point Absorber

For the single-tether asymmetric mass point absorber case, at the nominal buoy pose, optimal PTO stiffness is dependent on both the incident wave frequency and the tether length. The eigenvectors and eigenvalues of the system are calculated from the stiffness and mass matrices shown in Equation (6), where the optimal PTO stiffness is obtained for each wave frequency, and tether length is constrained to the range of 1-10 times the buoy radius. Results of the eigenanalysis for the asymmetric mass point absorber are shown in Figure 7, at a single incident wave frequency of $\omega = 0.45$ rad/sec, where the dashed vertical line represents the optimal tether length to buoy radius ratio at this frequency. Figure 7a shows the natural frequencies of the modes in rad/s. Due to strong coupling between surge and heave motion, mode 1 and mode 3 no longer represent a surge mode and a heave mode respectively. It can be seen that when tether length is increased, mode 1 changes from a heave-dominant mode to a surge-dominant mode, while mode 3 changes from a surge-dominant mode to a heave-dominant mode. The natural frequency of the heave-dominant mode remains approximately constant and is approximately equal to the wave frequency of 0.45 rad/sec, independent of the tether length. The natural frequency of surge-dominant mode decreases with the increase of tether length to radius ratio due to the fact that surge-dominant mode is governed by the pendulum motion of the buoy-tether system. The natural frequency of the pitch-dominant mode is higher than the normal incident wave frequency range and therefore is not shown here. It is clear that at a tether length to buoy radius ratio of approximately 4, the natural frequencies of the two modes are very close but not equal, which indicates the two modes are not resonant simultaneously for the optimal case.

Figure 7b shows the eigenvector of each oscillating mode. It is clear that at high tether length to buoy radius ratio, the eigenvector is similar to the generic single-tether case, where the modes are loosely coupled. However, under optimal conditions (at optimal tether length to buoy radius ratio of 4), the modes are strongly coupled (e.g. the off-diagonal terms and diagonal terms have similar modal components), indicating that maximum wave power can be absorbed in the Cartesian space of the buoy. The Cartesian space modal shapes at the optimal tether length are illustrated in Figure 8. It is clear that mode 1 and mode 3 oscillate diagonally in the Cartesian space of the buoy with an orthogonal relationship, which is rotated by 45° compared to standard heave and surge modal behavior observed from the generic single-tether point absorber. Figure 7c shows the normalized contributions to the tether velocity from each mode. It can be seen that for the asymmetric mass WEC, both the two orthogonal coupled modes lead to tether elongation. More specifically, contribution from mode 1 decreases with the increase of tether length, while contribution from mode 3 has the opposite trend. This implies that there is an optimal tether length that balances the contributions of the modes to the tether elongation velocity, which allows the single-tether asymmetric mass point absorber to absorb maximum power from the wave.

Figures 9a and 9b respectively show the optimal natural frequencies of the modes and optimal tether to buoy radius ratio against a range of feasible incident wave frequencies. The PTO setting as well as the tether length are optimized for the frequency-domain model given by Equations (3) and (6) for each wave frequency, with an initial tether length of 3.5m and an initial PTO setting optimal for the heave mode only (computed analytically from the heave equation of motion in the same manner like the generic single-tether case). The natural frequency of the pitch-dominant mode is always out of the possible incident wave frequency range and therefore is not shown here. It can be seen that the natural frequency of mode 3 is approximately equal to the wave frequency for the entire frequency range. The curve for mode 1 can be divided at 0.87 rad/s into two regions based on constrained tether length. Below 0.87 rad/s where tether length is optimized without reaching its length constraint, mode 1 diverges from its resonance condition with an increase in wave frequency. This implies that the resonance conditions for the two orthogonal coupled modes can not be achieved simultaneously, especially at higher wave frequencies, and therefore the system is not able to absorb all the power from the incident wave. Above 0.87 rad/s where tether length is restricted at the minimal allowed value (2.5m), the two modes can no longer oscillate along axes that are near 45° with respect to the global frame of the buoy, and consequently the modal behavior of the system approaches the generic single-tether case, where only the heave-dominant mode is tuned to resonance. In order to have two orthogonal coupled modes oscillating at higher frequencies, the mass of the buoy must be reduced to increase the natural frequency of the pendulum like motion of the buoy-tether system.

In comparison to the generic case, the asymmetric mass case allows the system to absorb power from both surge and heave modes and therefore in theory has the potential to absorb up to three times more power. In practice, however, for a range of wave frequencies, the physical constraints and control of the nominal tether length play an important role. The use of a fixed nominal tether length only allows the maximum power from wave to be absorbed at a single wave frequency, so consequently is sub-optimal for all other frequencies.

3.3 Three Tether Point Absorber

For the three-tether point absorber case, at the nominal buoy pose, the optimal PTO stiffness is dependent on both the incident wave frequency and the nominal tether inclination angle, α. The eigenvectors and eigenvalues are calculated from the stiffness and effective mass matrices shown in Equation (8), where the optimal PTO stiffness is obtained for each wave frequency, and tether angle, α, is selected between 0 and 90 degrees. Figure 10 shows the eigenanalysis results against tether angle at a single incident wave frequency of $\omega = 0.45$ rad/sec, where the dashed vertical line marks the optimal tether angle at this frequency. In Figure 10a, it can be seen that the natural frequency of the heave-dominant mode decreases with an increase in tether angle, while the natural frequency of the surge-dominant mode is a constant, approximately equal to the wave frequency of 0.45 rad/sec. The intersection of the two curves occur at the optimal

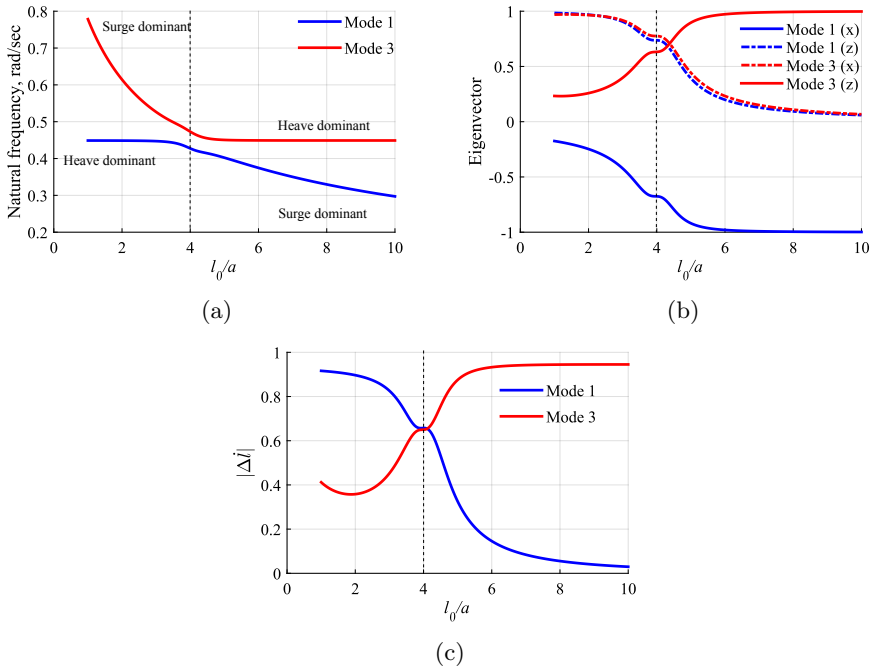

Figure 7: Eigenanalysis of the single-tether WEC with asymmetric mass distribution vs. tether nominal length for one incident wave frequency of $\omega = 0.45$ rad/sec: (a) Natural frequencies (eigenvalues) of buoy Cartesian space modes in rad/s; (b) Mode shapes (eigenvectors); (c) Contribution of the buoy Cartesian space modes to the tether velocity, $|\Delta \dot{l}|$.

tether angle of 54 degrees, derived in [17], at which both modes oscillate at the wave frequency, and consequently maximum wave power can be absorbed in the Cartesian space of buoy. The natural frequency of the pitch-dominant mode is higher than the incident wave frequency range considered and therefore is not shown here. The eigenvectors (modal components of the three-tether case) are shown in Figure 10b, where it is evident that the modes are loosely coupled, similar to generic single-tether case. Results of tether velocity arising from unit excitation of each mode vs tether angle are displayed in Figure 10c, where it can be seen that both the surge-dominant mode and the heave-dominant mode contribute to the tether movement. More specifically, contribution from the surge-dominant mode increases with an increase in tether angle, while contribution from the heave-dominant mode has the opposite trend. This implies that there is an optimal tether angle (54 degree for this wave frequency) that balances the contributions of the two translational modes to the tether elongation velocity, which allows the three-tether point absorber to absorb maximum power from the wave.

Figures 11a and 11b respectively show the optimal natural frequencies of

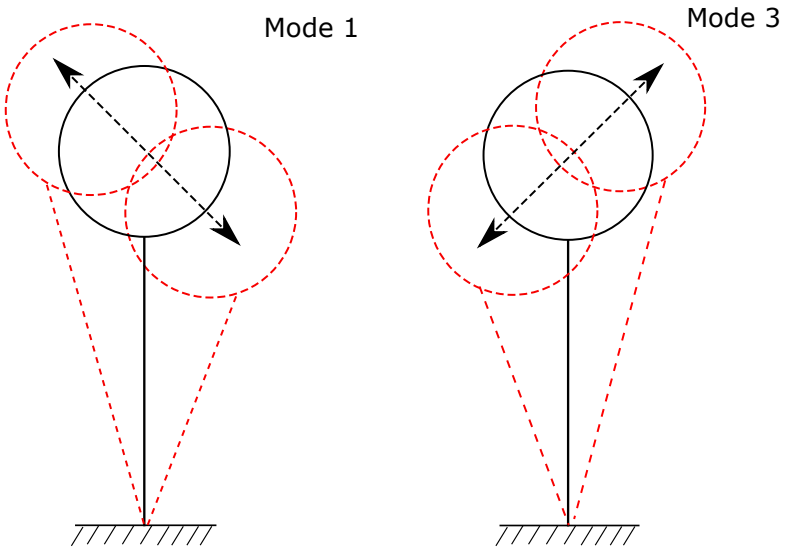

(a) Mode 1 (b) Mode 3

Figure 8: The mode shapes at optimal tether length to buoy radius ratio for wave frequency of 0.45 rad/s,

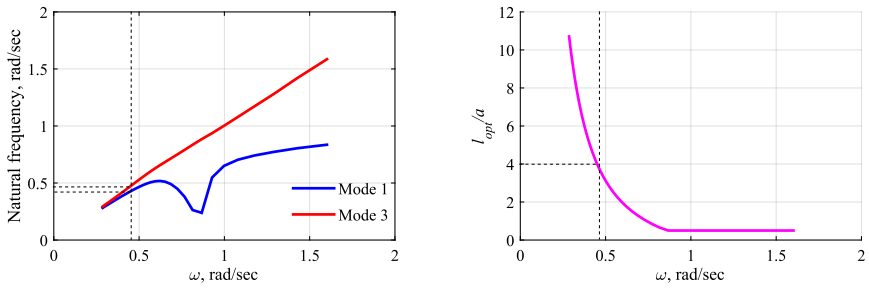

(a) (b)

Figure 9: (a) Natural frequencies of the single-tether WEC with asymmetric mass distribution against a range of incident wave frequencies at optimal conditions (optimal PTO setting and optimal nominal tether length for each frequency); (b) Optimal tether to buoy radius ratio against incident wave frequencies

modes and optimal tether angle against a range of incident wave frequencies. The PTO setting, as well as the tether angle, are optimized for the frequency-domain model given by Equation (3) with stiffness and effective mass matrices defined in Equation (8) for each wave frequency. The initial tether angle and initial PTO setting were optimal for the surge mode only (computed analytically

from the buoy surge motion of equation) [17]. From Figure 11a, it can be seen that the natural frequency of pitch-dominant mode is always out of the possible incident wave frequency range. The natural frequency of the surge-dominant mode is approximately equal to the incident wave frequency for the entire frequency range and therefore surge mode resonance is always achieved through PTO optimization. The natural frequency of the heave-dominant mode is very close to the incident wave frequency, except at wave frequencies higher than 1 rad/s (e.g. equivalent to 6.3s wave period). This implies that the three-tether point absorber has the potential to absorb almost all the power from waves at almost all possible wave frequencies. In addition, the results in Figure 11b indicate that the optimal tether angle is not overly sensitive to wave frequency, with optimal tether angle varying by less than 3 degree, which further implies that only a small amount of power could be lost in practice when the nominal tether angle is fixed. Both findings match the conclusions presented in [17].

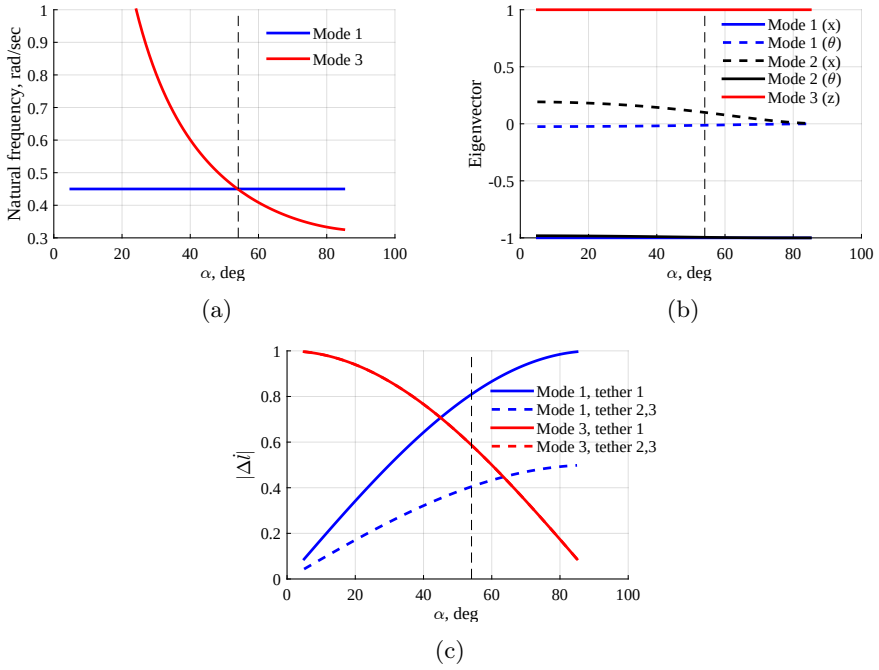

Figure 10: Eigenanalysis of the three-tether WEC vs. tether inclination angle, α, for one incident wave frequency of $\omega = 0.45$ rad/sec: (a) Natural frequencies (eigenvalues) of buoy Cartesian space modes; (b) Mode shapes (eigenvectors); (c) contribution of the buoy Cartesian space modes to the tether velocities, $|\,\Delta\dot{l}\,|$.

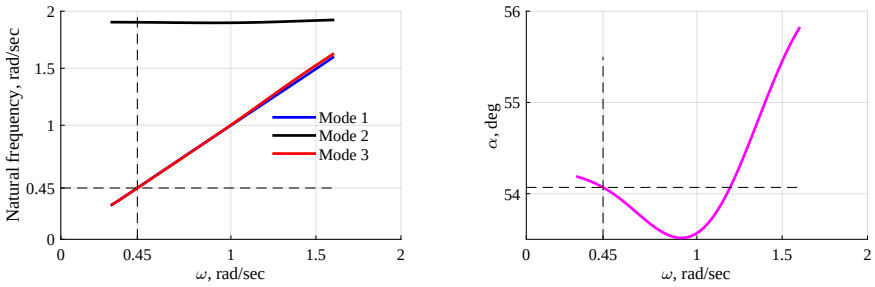

(a) (b)

Figure 11: : (a) Natural frequencies of the three-tether WEC against a range of incident wave frequencies at optimal conditions (optimal PTO setting and optimal nominal tether angle for each frequency); (b) Optimal tether angle against incident wave frequencies.

4 Discussion

From the eigenanalysis, it is clear that the generic single-tether point absorber case can only absorb energy from the heave-dominant mode, resulting in a maximum of one third of the wave power to be absorbed. This is due to the kinematic constraint of the single tether mechanism. Therefore, the surge-dominant mode and tether length do not play an important role in power absorption for this configuration.

For the single tether point absorber with asymmetric mass buoy, the concept was to enhance coupling between heave and surge modes in the buoy Cartesian space, thus allowing energy in surge to be transfered to heave, where it can be extracted effectively by the PTO. In this case, the nominal tether length plays an important role in terms of tuning the two primary modes associated with surge and heave motions towards resonance and also to be spatially orthogonal to each other oscillating near 45° with respect to the global frame of the buoy. At the optimal tether length, these two spatially-orthogonal surge-heave modes are strongly coupled, leading to roughly equal contribution to tether length velocity. Furthermore the natural frequencies of these modes are similar and are close to the incident wave frequency. In this study, the point mass to sphere mass ratio and mass offset have been kept at constant for simplicity, although these parameters also affect the modal behavior of the asymmetric mass buoy case. In practice, when experiencing varying wave conditions, the mass ratio, mass offset, tether length, and PTO setting are required to vary to absorb maximum power from waves. However, it is difficult to design a point absorber that allows the tuning of the first three parameters. With a fixed mass offset, mass ratio and tether length, the asymmetric mass plant is superior to a generic single-tether plant only for a narrow bandwidth of wave frequencies. However, if the natural frequencies are tuned to the peak in wave power spectra, then this plant will generate considerably more power than the generic single-tether case.

For the three-tether point absorber, the concept was to enhance the coupling between buoy modes and tether movement via an improved kinematic arrangement of the tethers, in order to absorb power from both the surge-dominant and the heave-dominant modes. In comparison to the asymmetric mass plant, the three-tether plant is superior in terms of achieving resonance conditions for both surge and heave-dominant modes, requiring small variation for the optimal tether angle over the entire feasible wave frequency range. This implies that the three-tether plant is more robust in practice and can absorb almost all the power from waves for the entire wave frequency range, with a constant nominal tether angle. More information on the three-tether point absorber and its optimal tether angle for various point absorber design is provided in [17].

In additional to the eigenanalysis, this study briefly compares the relative capture width (RCW) of the three point absorber variants for a range of wave frequencies, with and without tether elongation constraints, as shown in Figure 12. The constraint criteria proposed by Pizer [20] defines the wave amplitude $0.2a$ and tether elongation constraints $0.25a$ for the generic case. However, for the asymmetric mass case, the tether elongation needs to be sufficiently large to demonstrate its efficiency, and therefore $0.5a$ tether elongation constraints are used for this comparison study. The results are obtained from the frequency-domain models of the point absorber variants, linearized at the nominal pose of the point absorber, with PTO settings, tether length/angle optimized for each wave frequency. Since non-linear viscous damping cannot be modelled in the frequency-domain model, the lightly-damped surge motion of the single tether buoy is observed, leading to excessive coupled pitch motion for the asymmetric mass case during constrained optimization. Therefore, an additional linear damping is introduced on both the heave and surge modes, in order to ensure optimization stability and consequently to ensure the fidelity of the optimization results. Such additional "linearized viscous damping" has been numerically determined from the nonlinear viscous (drag) damping term behavior in a time-domain model (not discussed in this paper) of the asymmetric point absorber at 0.45 rad/s and is equally applied to all three point absorber variant models for a fair comparison under constrained optimization. The fixed parameters are defined as the same as shown in Table 2.

Relative capture width results for the three systems are shown in Figure 12, where it is clear that for the unconstrained case (represented by the dashed lines), the RCW of the three-tether point absorber is three times that of the generic single-tether point absorber, indicating that three-tether point absorber can absorb all the power from the wave for the entire frequency range. The RCW of the asymmetric mass point absorber varies from near that of the three-tether case at lower wave frequencies to near that of the generic single-tether case at higher wave frequencies. This decreasing trend is associated with the bounding of the search space for the nominal tether length (tether length is not allowed to be shorter than 2.5m). When nominal tether length reaches its minimal allowed value, the two coupled surge-heave modes can no longer remain at an angle of near 45° with respect to the global frame of the buoy as shown in Figure 8, and consequently the behavior of the asymmetric mass

point absorber approaches the generic single-tether point absorber. With a tether elongation constraint of $0.5a$ (results presented by the solid lines), the three-tether point absorber is about 2.5 to 3 times more efficient than the generic single-tether point absorber. The RCWs for the three systems do not converge to the unconstrained results at higher frequency due to the impact of the additional "linearized viscous damping" terms. Such impact is more significant for the three-tether case due to the fact that three-tether point absorber absorbs power from both surge and heave modes and consequently the added viscous damping dissipates nearly double the power dissipated in the asymmetric mass system. The RCW of the asymmetric mass point absorber with the tether elongation constraint is up to two times that of the generic single-tether point absorber. It is surprising that with the same tether elongation constraints, the RCW of the asymmetric mass point absorber is even higher than the RCW of the three-tether point absorber at wave periods greater than 8s (below 0.75 rad/s). This behavior is very likely to be associated with hydrodynamic coefficients of the buoy, however, deeper investigation is required to understand the reasons behind this.

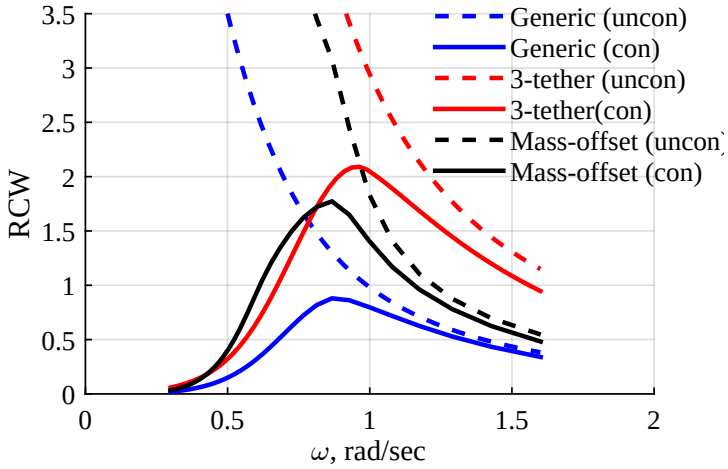

Figure 12: RCW of the point absorber variants (blue lines for the generic single-tether case; black lines for the asymmetric mass case; red lines for the three-tether case) with and without tether elongation constraints over the entire feasible wave frequency range (wave amplitude is $0.2a$, the maximum tether elongation is constraint by $0.5a$). Dashed lines represent the theoretical maximum of the RCW for each point absorber variant (without tether elongation constraint); Solid lines represent the results with the tether elongation constraint of $0.5a$.

5 Summary

This paper investigated three spherical submerged point absorber variants to understand the behavior of these systems from a modal perspective using eigenanalysis. Results show that in theory, both the asymmetric mass point absorber and three-tether point absorber have the potential to absorb two to three times more energy in comparison to the generic single-tether spherical point absorber. However, there are some trade-offs to consider in the design process. For the generic buoy, there is one tunable parameter, namely the PTO stiffness, and making this frequency dependent can keep the heave mode resonant for any incident wave frequency. For the asymmetric mass spherical point absorber, there are two modes that need to be close to resonance in order to achieve optimal power extraction. The PTO stiffness provides one independent tuning parameter. The other must come from one of the physical parameters of the system, namely the mass and mass distribution, buoyancy and the tether length. If optimal conditions are to be achieved for a range of sea states, then control of one or more of these physical parameters is necessary in real-time to broaden the resonance bandwidth of the system. Furthermore, for the same PTO stroke, the asymmetric mass point absorber absorbs more power via generating more useful force on the PTO in comparison to the generic single-tether case, and therefore a PTO system with a higher loading capacity is necessary, leading to a higher cost to manufacture the PTO. By contrast, three-tether point absorber is more robust and is able to absorb almost all the energy from the incident wave when only PTO control is applied. However, the cost of introducing an additional two PTO systems can be significant. Future work will focus on control investigation and techno-economic assessments of these two variants.

References

[1] J. Hals, J. Falnes, and T. Moan, "Constrained optimal control of a heaving buoy wave-energy converter," *Journal of Offshore Mechanics and Arctic Engineering*, vol. 133, no. 1, pp. 1–15, 2010.

[2] J. V. Ringwood, G. Bacelli, and F. Fusco, "Energy-maximizing control of wave-energy converters: the development of control system technology to optimize their operation," *Control Systems, IEEE*, vol. 34, no. 5, pp. 30–55, 2014.

[3] J. Hayward and P. Osman, "The potential of wave energy," report, CSIRO, 2011.

[4] G. Mork, S. Barstow, A. Kabuth, and M. T. Pontes, "Assessing the global wave energy potential," in *Proceedings of ASME 2010 29th International Conference on Ocean, Offshore and Arctic Engineering*, (Shanghai, China), pp. 447–454, American Society of Mechanical Engineers, 2010.

[5] M. McCormick, *Ocean Wave Energy Conversion*. Wiley, 1981.

[6] The European Marine Energy Centre, "Wave devices," n.d. Accessed 15 January 2015,
http://www.emec.org.uk/marine-energy/wave-devices/.

[7] B. Drew, A. R. Plummer, and M. N. Sahinkaya, "A review of wave energy converter technology," *Proceedings of the Institution of Mechanical Engineers, Part A: Journal of Power and Energy*, vol. 223, no. 8, pp. 887–902, 2009.

[8] J. Cruz, *Ocean wave energy: Current status and future prespectives*. Green Energy and Technology, Berlin: Springer Berlin Heidelberg, 2008.

[9] K. Budal and J. Falnes, "A resonant point absorber of ocean-wave power," *Nature*, vol. 256, no. 5517, pp. 478–479, 1975.

[10] D. V. Evans, "A theory for wave-power absorption by oscillating bodies," *Journal of Fluid Mechanics*, vol. 77, no. 1, pp. 1–25, 1976.

[11] J. N. Newman, *Marine Hydrodynamics*. MIT press, 1977.

[12] J. Falnes, *Ocean waves and oscillating systems: Linear interactions including wave-energy extraction*. Cambridge University Press, 2002.

[13] W. E. Cummins, "The impulse response function and ship motions," report, DTIC Document, 1962.

[14] A. Babarit, J. Hals, M. Muliawan, A. Kurniawan, T. Moan, and J. Krokstad, "Numerical estimation of energy delivery from a selection of wave energy converters – final report," report, Ecole Centrale de Nantes & Norges Teknisk-Naturvitenskapelige Universitet, 2011.

[15] A. Babarit and A. H. Clement, "Optimal latching control of a wave energy device in regular and irregular waves," *Applied Ocean Research*, vol. 28, no. 2, pp. 77–91, 2006.

[16] M. A. Srokosz, "The submerged sphere as an absorber of wave power," *Journal of Fluid Mechanics*, vol. 95, no. 4, pp. 717–741, 1979.

[17] N. Y. Sergiienko, B. S. Cazzolato, B. Ding, and A. Maziar, "An optimal arrangement of mooring lines for the three-tether submerged point-absorbing wave energy converter," *Renewable Energy*, vol. 93, no. 2016, pp. 27–37, 2016.

[18] S. M. Lattanzio and J. T. Scruggs, "Maximum power generation of a wave energy converter in a stochastic environment," in *Proceedings on IEEE International Conference on Control Applications (CCA), 2011*, (Denver, CO), pp. 1125–1130, IEEE, 2011.

[19] J. T. Scruggs, S. M. Lattanzio, A. A. Taflanidis, and I. L. Cassidy, "Optimal causal control of a wave energy converter in a random sea," *Applied Ocean Research*, vol. 42, no. 2013, pp. 1–15, 2013.

[20] D. J. Pizer, "Maximum wave-power absorption of point absorbers under motion constraints," *Applied Ocean Research*, vol. 15, no. 4, pp. 227–234, 1993.

[21] P. C. Vicente, A. F. Falco, and P. A. Justino, "Nonlinear dynamics of a tightly moored point-absorber wave energy converter," *Ocean Engineering*, vol. 59, pp. 20 – 36, 2013.

6 Appendix

In this section, the motion equations of asymmetric mass buoy (shown in Figure 2) is derived in frequency domain. As the fluid drag force is quadratic with respect to velocity, this term is neglected in this model. This simplification does not significantly influence the result of modal analysis, since for a buff body with a large dimension compared to wave amplitude, the wave inertia force is dominant [11]. This linearisation method was developed from the approach used in [21], with the same condition of small wave amplitude ($A_m = 0.1$m). The equation of motion in the frequency-domain is re-written as

$$(\mathbf{M} + \mathbf{A}(\omega))\hat{\ddot{\mathbf{x}}} + (\mathbf{B}(\omega))\hat{\dot{x}} = \hat{\mathbf{F}}_{exc} + \hat{\mathbf{F}}_{h/stat} + \hat{\mathbf{F}}_{pto}, \tag{10}$$

where $\mathbf{A}(\omega)$ and $\mathbf{B}(\omega)$ are added mass matrix and damping coefficient matrix respectively, and $\hat{\mathbf{F}}_{exc}$, $\hat{\mathbf{F}}_{h/stat}$, and $\hat{\mathbf{F}}_{pto}$ are the wave excitation force, hydrostatic, and PTO forces exerted on the body respectively.

As shown in Figure 2, $z_2 = r_{gy}\sin(\varphi - \theta)$ and $x_2 = r_{gy}\cos(\varphi - \theta)$. The mass matrix, $\mathbf{M}$, can be expressed as

$$\mathbf{M} = \begin{pmatrix} m_1 + m_2 & 0 & m_2 r_{gy}\sin(\varphi-\theta) \\ 0 & m_1 + m_2 & -m_2 r_{gy}\cos(\varphi-\theta) \\ m_2 r_{gy}\sin(\varphi-\theta) & -m_2 r_{gy}\cos(\varphi-\theta) & I_y \end{pmatrix},$$

in which m_1 is the mass of spherical buoy, m_2 is the offset point mass, and I_y is the total moment of inertia of the buoy about its geometric center.

The small wave amplitude, A_m, leads to the small pitch motion θ. The mass matrix can be approximated as

$$\mathbf{M} = \begin{pmatrix} m_1 + m_2 & 0 & m_2 r_{gy}\sin(\varphi) \\ 0 & m_1 + m_2 & -m_2 r_{gy}\cos(\varphi) \\ m_2 r_{gy}\sin(\varphi) & -m_2 r_{gy}\cos(\varphi) & I_y \end{pmatrix}. \tag{11}$$

The hydrostatic force is

$$\hat{\mathbf{F}}_{h/stat} = \begin{pmatrix} 0 \\ \rho V g - (m_1 + m_2)g \\ m_2 g r_{gy}\cos(\varphi - \theta) \end{pmatrix} \approx \begin{pmatrix} 0 \\ \rho V g - (m_1 + m_2)g \\ m_2 g r_{gy}(\cos(\varphi) + \sin(\varphi)\theta) \end{pmatrix}, \tag{12}$$

in which the V is the volume of spherical buoy, equal to $4/3\pi a^3$.

The vector $\hat{\mathbf{F}}_{ex}$ is composed of surge and heave wave excitation force amplitude,

$$\hat{\mathbf{F}}_{ex} = \begin{pmatrix} F_{ex,x} \\ F_{ex,z} \\ 0 \end{pmatrix}, \tag{13}$$

where the excitation force in pitch is zero because here a spherical buoy has been used.

The PTO force is expressed as

$$\hat{\mathbf{F}}_{pto} = (-C_{pto} - B_{pto}\Delta\dot{l} - K_{pto}\Delta l)\mathbf{T}, \tag{14}$$

in which $\mathbf{T}$ is the transformation matrix which transforms the PTO force and torque into the positive x, y and z axis of global frame. C_{pto} is given by Equation (2).

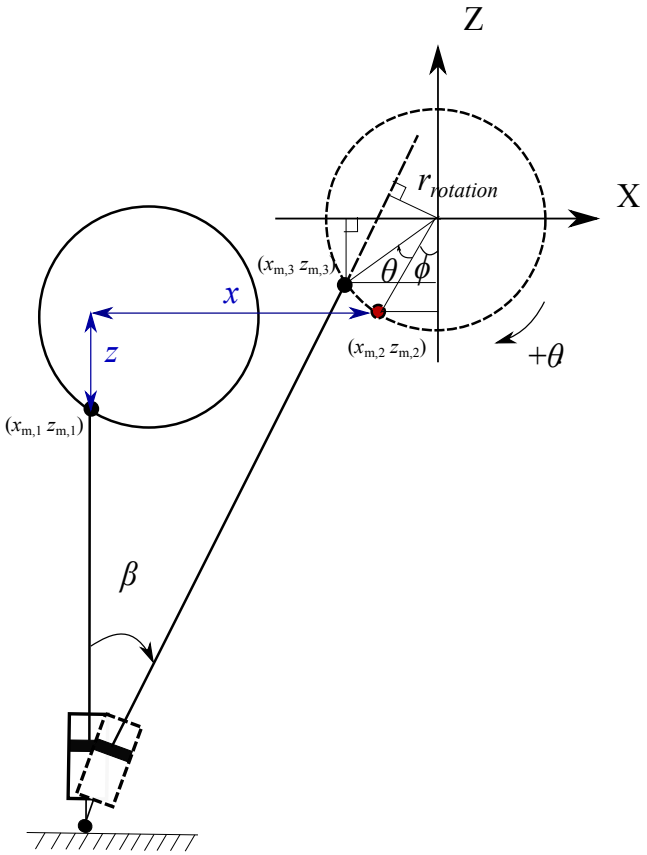

Figure 13: Generic single tether fully submerged point absorber

As illustrated in Figure 13, when the buoy moves to an arbitrary position, and assuming that the mooring point $(x_{m,1}, z_{m,1})$ was initially translated to $(x_{m,2}, z_{m,2})$ and then rotated by an angle of θ, the change in the PTO extension Δl is given by

$$\Delta l = \sqrt{(l_0 + z + a\cos(\phi) - a\cos(\phi+\theta))^2 + (x + a\sin(\phi) - a\sin(\phi+\theta))^2} - l_0, \tag{15}$$

in which x and z represent the displacement with respect to the x and z global frame respectively, and θ is the angle with y axis in the global frame.

As the angle θ is small, $\cos(\theta) \approx 1$ and $\sin(\theta) \approx \theta$, Eqn (15) can be simplified to

$$\Delta l \approx \sqrt{(l_0 + z + a\sin(\phi)\theta)^2 + (x - a\cos(\phi)\theta)^2} - l_0. \tag{16}$$

As $l_0 \gg x$ for small wave amplitudes, $l_0 + z - a\sin(\phi)\theta \gg x - a\cos(\phi)\theta$, hence the PTO extension is given by

$$\Delta l \approx z + a\sin(\phi)\theta. \tag{17}$$

The hydrostatic force used to balance the net buoyancy is given by

$$C_{pto} = \rho V g - (m_1 + m_2)g. \tag{18}$$

For the transformation vector $\mathbf{T}$,

$$\mathbf{T} = \begin{pmatrix} \sin(\beta) \\ \cos(\beta) \\ r_{rotation} \end{pmatrix}, \tag{19}$$

in which, as the tether angle β is small, $\cos(\beta) \approx 1$ and $\sin(\beta)$ is given by

$$\sin(\beta) \approx \tan(\beta) = \frac{x - a\cos(\phi)\theta}{l_0 + z + a\sin(\phi)\theta}. \tag{20}$$

As $l_0 \gg z - a\sin(\phi)\theta$ for small wave amplitude, Eqn (20) can be approximated as

$$\sin(\beta) \approx \frac{x - a\cos(\phi)\theta}{l_0}. \tag{21}$$

The instantaneous distance, $r_{rotation}$, as shown in Figure 13 is given by

$$\begin{aligned} r_{rotation} &= a\sin(\phi + \theta - \beta) \\ &= a(\sin(\phi + \theta)\cos(\beta) - \cos(\phi + \theta)\sin(\beta)) \\ &\approx a(\sin(\phi) + \cos(\phi)\theta - \cos(\phi)\frac{x - a\cos(\phi)\theta}{l_0}). \end{aligned} \tag{22}$$

Substituting Eqn (11)-(22) into Eqn (10), gives

$$
\begin{pmatrix} m_1+m_2+a_{11} & 0 & m_2 r_{gy}\sin(\varphi) \\ 0 & m_1+m_2+a_{33} & -m_2 r_{gy}\cos(\varphi) \\ m_2 r_{gy}\sin(\varphi) & -m_2 r_{gy}\cos(\varphi) & I_y \end{pmatrix} \begin{pmatrix} \ddot{x} \\ \ddot{z} \\ \ddot{\theta} \end{pmatrix} + \begin{pmatrix} b_{11} & 0 & 0 \\ 0 & b_{33} & 0 \\ 0 & 0 & 0 \end{pmatrix} \begin{pmatrix} \dot{x} \\ \dot{z} \\ \dot{\theta} \end{pmatrix}
$$
$$
= \begin{pmatrix} F_{ex,x} - C_{pto}\frac{x - a\cos(\phi)\theta}{l_0} \\ F_{ex,z} - (K_{pto}(z + a\sin(\phi)\theta) + B_{pto}(\dot{z} + a\sin(\phi)\dot{\theta}) \\ \begin{pmatrix} -C_{pto}a(\sin(\phi) + \cos(\phi)\theta - \cos(\phi)\frac{x - a\cos(\phi)\theta}{l_0}) - K_{pto}a(z + a\sin(\phi)\theta)\sin(\phi) \\ -B_{pto}a(\dot{z} + a\sin(\phi)\dot{\theta})\sin(\phi) + m_2 g r_{gy}(\cos(\varphi) + \sin(\varphi)\theta) \end{pmatrix} \end{pmatrix}. \tag{23}
$$

Re-arranging Eqn(6),

$$
\begin{pmatrix} m_1+m_2+a_{11} & 0 & m_2 r_{gy}\sin(\varphi) \\ 0 & m_1+m_2+a_{33} & -m_2 r_{gy}\cos(\varphi) \\ m_2 r_{gy}\sin(\varphi) & -m_2 r_{gy}\cos(\varphi) & I_y \end{pmatrix} \begin{pmatrix} \ddot{x} \\ \ddot{z} \\ \ddot{\theta} \end{pmatrix}
$$
$$
+ \begin{pmatrix} b_{11}(\omega) & 0 & 0 \\ 0 & b_{33}(\omega) + B_{pto} & B_{pto}a\sin(\phi) \\ 0 & B_{pto}a\sin(\phi) & B_{pto}a^2\sin^2(\phi) \end{pmatrix} \begin{pmatrix} \dot{x} \\ \dot{z} \\ \dot{\theta} \end{pmatrix}
$$
$$
+ \begin{pmatrix} C_{pto}/l_0 & 0 & -C_{pto}a\cos(\phi)/l_0 \\ 0 & K_{pto} & K_{pto}a\sin(\phi) \\ -C_{pto}a\cos(\phi)/l_0 & K_{pto}a\sin(\phi) & \begin{pmatrix} C_{pto}a\cos(\phi) - m_2 g r_{gy}\sin(\varphi) \\ +C_{pto}a^2\cos^2(\phi)/l_0 + K_{pto}a^2\sin^2(\phi) \end{pmatrix} \end{pmatrix} \begin{pmatrix} x \\ z \\ \theta \end{pmatrix}
$$
$$
= \begin{pmatrix} F_{ex,x} \\ F_{ex,z} \\ 0 \end{pmatrix}. \tag{24}
$$